

Data augmentation experiments with style-based quantum generative adversarial networks on trapped-ion and superconducting-qubit technologies

Julien Baglio

QuantumBasel, Schorenweg 44B, CH-4144 Arlesheim, Switzerland.

E-mail: julien.baglio@quantumbasel.com

Abstract. In the current noisy intermediate scale quantum computing era, and after the significant progress of the quantum hardware we have seen in the past few years, it is of high importance to understand how different quantum algorithms behave on different types of hardware. This includes whether or not they can be implemented at all and, if so, what the quality of the results is. This work quantitatively demonstrates, for the first time, how the quantum generator architecture for the style-based quantum generative adversarial network (qGAN) can not only be implemented but also yield good results on two very different types of hardware for data augmentation: the IBM `ibm_torino` quantum computer based on the Heron chip using superconducting transmon qubits and the `aria-1` IonQ quantum computer based on trapped-ion qubits. The style-based qGAN, proposed in 2022, generalizes the state of the art for qGANs and allows for shallow-depth networks. The results obtained on both devices are of comparable quality, with the `aria-1` device delivering somewhat more accurate results than the `ibm_torino` device, while the runtime on `ibm_torino` is significantly shorter than on `aria-1`. Parallelization of the circuits, using up to 48 qubits on IBM quantum systems and up to 24 qubits on the IonQ system, is also presented, reducing the number of submitted jobs and allowing for a substantial reduction of the runtime on the quantum processor to generate the total number of samples.

Keywords: quantum machine learning, data augmentation, generative adversarial models, quantum hardware implementation, trapped-ion qubits, superconducting qubits

1. Introduction

Quantum computing has seen great progress happening in the past few years, and is now starting a shift from very early stages focused on hardware progress to more focused use-case studies and applications. The current state of the art for the quantum hardware is still that of the noisy intermediate-scale quantum (NISQ) computers, characterized by a low number of qubits (of the order of maximally 1000 qubits for gate-based architectures, 5000 for quantum annealers, as of early 2024) and with capabilities limited by the noise of the hardware and by the low number of couplers between the qubits. Despite these limitations, the first advances toward quantum computational supremacy were shown for superconducting processors in 2019 [1], photonic approaches in 2020 and 2022 [2, 3], and in 2023 claims for quantum utility were presented in Ref. [4] on IBM 127-qubit processors. Substantial improvement in encoding logical qubits have been presented in Ref. [5] (with neutral atoms) and Ref. [6] (with trapped-ion qubits), a new quantum error correction protocol with substantial improvement has been presented in Ref. [7] and very recently a claim for quantum supremacy using quantum annealing has been presented in Ref. [8] after several advancements in that direction [9, 10]. These results have in turn boosted the research in classical tensor network architectures, see for example Refs. [11–14], advancing both the field of classical and quantum algorithms.

Amongst the various algorithms designed for the NISQ era [15–17], quantum machine learning (QML) [18, 19] is of high interest given the range of real-world applications: financial services, healthcare, high energy physics, just to name a few [20]. We focus in this paper on quantum generative models [21–25], in particular quantum

generative adversarial networks (qGANs) [26–34], for a recent review see Ref. [35]. These quantum architectures belong to the general class of quantum neural networks, or parameterized quantum circuits [36–39]. Trainability of qGANs has been studied [40, 41] and in particular Ref. [41] indicates that qGANs with shallow circuits for their quantum generator do not suffer from barren plateaus, making them promising tools for generative applications. We are in particular interested by data augmentation: A model is trained with a small amount of input samples and it learns how to sample the underlying distribution. This is particularly interesting in the financial sector for filling gaps in time series [42–45], or in healthcare applications for which (good quality) datasets could be too small to be used for further training of another machine learning model [46–48]. Quantum GANs are also promising for generative drug discovery [49–51].

The quantum algorithm we have selected for data augmentation is the style-based qGAN which we have proposed with other colleagues in Ref. [33]. In the style-based qGAN, the latent variables of the quantum generator are repeatedly encoded over the entire quantum network and not only in the first quantum gates. This approach has been proven to generalize the standard qGANs [28, 30, 32, 52]. The data augmentation was demonstrated on real-world data provided by Monte Carlo event distributions typically encountered in particle physics at hadron colliders and which display highly non-Gaussian profiles [33]. Not only these type of distributions are a difficult playground for classical GANs in the context of data augmentation, but it has been shown that significantly smaller Kullback-Leibler (KL) divergences are achieved by the style-based qGAN compared to the standard qGAN.

There has been tremendous progress in the past few years in the deployment of NISQ gate-based hardware. The first type of hardware which has been accessible on the cloud is the superconducting qubit type provided by IBM [53], with publicly available devices up to 133 qubits as of early 2024[‡]. Google Sycamore processor [1] and Rigetti Ankaa class processors [54] are other examples of superconducting qubit types. Other types of quantum hardware, able to execute QML algorithms, have seen remarkable progress in the past few years and are also accessible via cloud providers or via direct cloud access from the hardware providers. The most commercially advanced quantum computers besides superconducting qubit technology are trapped-ion qubits [55], such as provided by IonQ [56], for which the current state-of-the-art device is Forte with 30 qubits [57] before the deployment of Forte Enterprise planned for end of 2024 with 35 (algorithmic) qubits and Tempo following after with 64 (algorithmic) qubits[§]; or provided by Quantinuum [58] for which the current state-of-the-art quantum processor is the 32-qubit H2 computer with the highest two-qubit gate fidelity of the market^{||}. Besides superconducting qubits and trapped-ion qubits, quantum computers based on photonic technology and on neutral atoms are also used for QML implementation [59–62], for which prominent companies are e.g. Xanadu, QuEra, or Pasqal. Given all

[‡] See the IBM quantum roadmap at <https://www.ibm.com/quantum/technology>.

[§] See for example this article in The Quantum Insider, June 2023.

^{||} See H2 processor specifications at <https://www.quantinuum.com/hardware/h2>.

this technical improvement, it is of great importance to understand how key quantum algorithms, such as qGANs, behave on different types of hardware. In particular, we are interested to test whether or not they can be implemented at all and, if so, what the quality of the results is. This also indicates what hardware improvements are required to improve the results. It can be expected that one- and two-qubit gate errors as well as readout errors play an important role, while coherence time is less important since the style-based qGAN circuits are usually shallow. It should be noted that error mitigation and error suppression techniques, such as provided by IBM or other quantum providers such as the `Fire Opal` tool from Q-CTRL, are also of great help to overcome the issues with hardware errors.

This work has two goals: (1) Assess quantitatively whether the style-based qGAN algorithm can perform good data augmentation on two different hardware architectures: superconducting qubits, as provided e.g. by IBM, and trapped-ion qubits as provided e.g. by IonQ. This was hinted in Ref. [33] but a quantitative study is still lacking. (2) Compare the performance on these two architectures, and highlight their respective advantages and drawbacks in the current NISQ era. Our results should be viewed as experimental quantum algorithm research: We want to compare trapped-ion and superconducting hardware technologies for the specific use case of data augmentation using style-based qGAN, in the same spirit as done for example in Ref. [63] for Heisenberg spin chain dynamics. We do not wish to characterize the performance of the algorithm *per se* or compare it to other (quantum or classical) generative models, as would be the work done e.g. in Refs. [64–66] for various quantum generative models. However we note that Ref. [65] indicates that quantum generative models can outperform classical models in the data-limited regime, which is precisely of high interest for data augmentation applications; see also Ref. [67] for a characterization of qGANs indicating the same conclusion. Because we want to compare the native hardware performance as best as we can, we do not use any error suppression nor error mitigation of the results. Such a study is important but goes beyond the scope of this work.

Compared to the work in Ref. [33] we also extend the algorithmic implementation of the style-based qGAN using the parallelization of the base ansatz, allowing us to perform our runs using up to 24 qubits on the `aria-1` IonQ system and up to 48 qubits on the `ibm_torino` quantum computer of IBM using the latest Heron quantum processor. This leads to a substantial reduction of the total time needed to obtain the total number of generated samples.

The paper is organized as follows. In Section 2 we present the two quantum computers on which we implement the style-based qGAN algorithm: the `ibm_torino` device based on the IBM Heron superconducting transmon qubits and the `aria-1` device based on the IonQ trapped-ion qubits. In Section 3 we summarize briefly the design and architecture of the style-based qGAN. We also introduce the parallelization allowing for reducing the number of effective runs required to obtain the total number of samples from the quantum generator. In Section 4 we present the experimental results of the hardware implementation in the context of data augmentation using Monte Carlo distributions

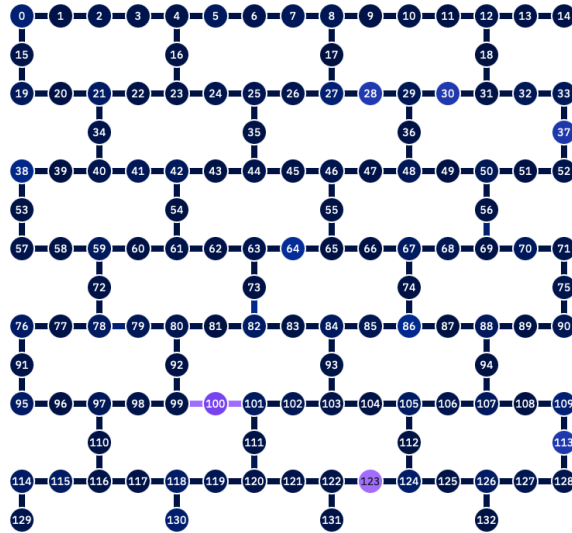


Figure 1. Qubit coupling map of the 133-qubit `ibm_torino` system based on the IBM Heron chip.

for high-energy physics as real-world data, comparing the performance of `aria-1` and of `ibm_torino`. In Section 5 we present our conclusion and outlook for further explorations. In Appendix Appendix A we include a noise simulation for the IonQ `aria-1` device comparing runs using 512 shots and 1024 shots, while Appendix Appendix B presents additional results on the IBM `ibm_cusco` device based on the Eagle chip.

2. Superconducting transmon and trapped-ion quantum computers

We have implemented the style-based qGAN algorithm on two different hardware technologies, namely superconducting transmon qubits as manufactured by IBM and trapped-ion qubits as manufactured by IonQ.

IBM uses superconducting transmon qubits [68, 69] for their quantum chip. The qubit is made out of a Josephson junction of the size of about 100 nm [70], acting as a nonlinear inductor, coupled with a shunting capacitor. This circuit creates an anharmonic oscillator. The qubits are cooled down to mK temperatures to enter the superconducting regime and exhibit quantized energy levels. The typical resonance frequency is around 5 GHz. Controlling of the qubits, including readout as well as gate operations, is performed thanks to microwave resonators coupled to the chip [71, 72]. We have used the `ibm_torino` quantum system which is the latest IBM prototype using the Heron architecture with 133 qubits. The qubit connectivity is defined by a heavy-hex lattice¶ and the Heron chip, which is the baseline for the new IBM System 2 system, is a substantial improvement over the previous Eagle chip with ten times better two-qubit gate fidelity⁺. The qubit coupling map for the `ibm_torino` quantum system using

¶ See this IBM blog post on heavy-hex lattice architecture.

⁺ See the different IBM quantum processor types in the IBM documentation.

| | <code>ibm_torino</code> | <code>aria-1</code> |
|--|-------------------------|----------------------|
| # of qubits | 133 | 25 |
| Coherence time T_1 (μs) | 157 | 10^8 |
| Coherence time T_2 (μs) | 140 | 10^6 |
| One-qubit gate time (μs) | 0.032 | 135 |
| Two-qubit gate time (μs) | 0.101^a | 600^b |
| Readout time (μs) | 1.56 | 300^c |
| One-qubit gate error rate | 5.8×10^{-4} | 3×10^{-4} |
| Two-qubit gate error rate | 5.3×10^{-3} | 6×10^{-3} |
| Readout error rate | 2.7×10^{-2} | 5.1×10^{-3} |

^aCZ gate; ^bMølmer-Sørensen gate; ^cOn all qubits at once.

Table 1. List of the most important parameters from the technical specifications of the IBM `ibm_torino` (left) and IonQ `aria-1` (right) devices (average values over all the qubits). The actual values change over time after each calibration of the system and reflect the specifications at the time of our experiments (for IBM system: December 13th, 2023; for IonQ system: spanned over mid-February to mid-March 2024).

the Heron chip is displayed in Figure 1 and the most important parameters from the technical specifications of the device are listed in Table 1.

Trapped-ion quantum computers use ionized atoms trapped with a laser [55]. IonQ quantum systems are currently based on ytterbium ions [56], $^{171}\text{Yb}^+$, confined on a chip called a linear ion trap, featuring around 100 electrodes producing the rapidly oscillating electromagnetic fields needed for the trap. The hyperfine transitions of the $^2S_{1/2}$ ground state are used as $|0\rangle$ and $|1\rangle$ qubit states. The ions are cooled by the lasers using a combination of Doppler and resolved sideband cooling. The initial state is prepared in the ground state $|0\rangle$ via optical pumping. One- and two-qubit gate operations are processed sequentially, using 355nm-pulsed Raman beams, SK1 pulses for one-qubit operations [73] and Mølmer-Sørensen interactions for two-qubit operations [74, 75]. The readout is performed on all ions at once, using a 369-nm laser resonant with the $^2S_{1/2} \rightarrow ^2P_{1/2}$ transition. The laser operations allow for an all-to-all connectivity of the qubits. We have used IonQ `aria-1` quantum system, with 25 qubits and the technical specifications as listed in Table 1 for the most important parameters.

It is quite instructive to compare the parameters in Table 1 for the two quantum computers `aria-1` and `ibm_torino`. Besides the very important difference in terms of connectivity, with all-to-all for the trapped-ion architecture vs the heavy-hex lattice for the superconducting transmon qubit architecture, the other salient differences lie in the coherence time, the one-qubit gate error and the readout error.

Trapped-ion qubits have a very long coherence time, $T_1 = 100$ s, compared to the typical coherence time of order $200 \mu\text{s}$ for superconducting transmon qubits. This has an impact on the number of gate operations that can be performed before measuring just noise: IonQ systems can run in principle deeper circuits, as evidenced by the T2-over-two-qubit-gate-time ratio which is of order 1400 on `ibm_torino` and of order 1700 on `aria-1`. The higher this ratio is, the more operations you can perform in a given quantum circuit before losing the whole quantum coherence. On the other hand,

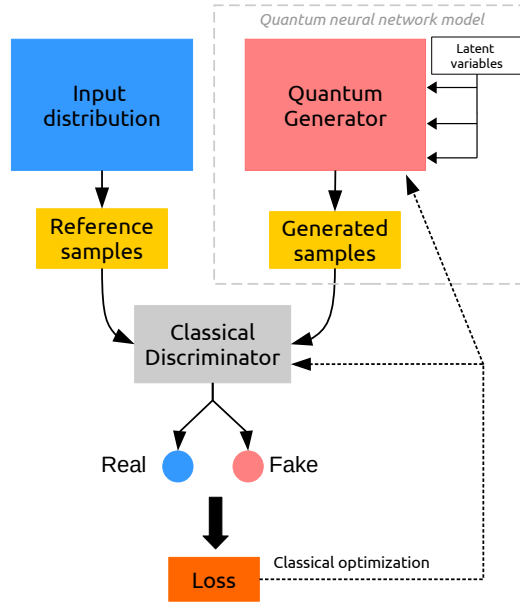


Figure 2. Workflow of a qGAN training where the discriminator uses a classical neural network while the generator is a quantum network. This is the setup of the style-based qGAN algorithm we use in this work. The generated samples out of the quantum generator are compared against the reference samples, the latter being taken from the input training data. Both generated and reference samples are used to train the discriminator, using an appropriate loss function for both the discriminator and the generator. The parameters of both networks are then updated and the procedure is repeated in an adversarial approach until desired precision is reached. The figure is taken from Ref. [33].

operations on `aria-1` take a much longer time compared to operations on `ibm_torino`, as there is a three-order-of-magnitude difference in the two-qubit gate operations time.

The two-qubit gate error rates are quite comparable, while the IonQ `aria-1` device has a significantly better readout fidelity than the IBM `ibm_torino` device, by one order of magnitude. We expect this readout fidelity to have more impact on the accuracy of our data augmentation experiment than the difference in coherent time between the two quantum devices, as our quantum circuits are quite shallow.

3. Style-based quantum GAN and parallelization

3.1. Workflow of a (quantum) GAN

We briefly present in this section how a GAN, be it classical or quantum, is implemented. A GAN contains two competing networks, the generator and the discriminator, which are trained alternately following an adversarial procedure [76]. The goal of the generator is to produce candidate data (or “fake data”) out of random noise input, while the goal of the discriminator is to distinguish the candidate data produced by the generator from the training data it is fed with (the “real data”).

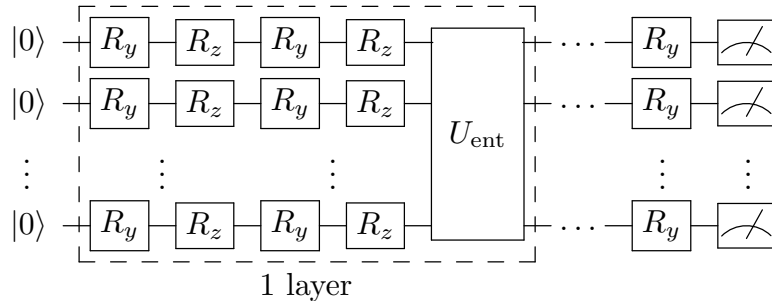


Figure 3. Ansatz for the quantum generator of the style-based qGAN. U_{ent} in our case stands for controlled R_z rotations. The figure is taken from [33].

The training procedure follows a zero-sum two-player game until (ideally) a Nash equilibrium is reached: the discriminator cannot discriminate between fake and real data better than randomly selecting true or false, and the parameters of the generators have now reached their final values so that the random input distribution of the generator is converted into realistic data by the network. The step from a classical GAN to a quantum GAN (qGAN) can be realized either by using a quantum architecture for the generator, or for the discriminator, or for both [26, 35]. Note that game-theory arguments indicate that a Nash equilibrium may not exist in all cases for GANs [77], related to the fact that the training of classical GANs may be challenging with, amongst other issues, vanishing gradients [78]. Interestingly this is another argument in favor of qGANs which, for example, are more likely to avoid the problem of vanishing gradients as indicated in Ref. [41] when the generator of the GAN is a quantum network.

The style-based qGAN algorithm uses the hybrid approach with a classical discriminator network and a quantum architecture for the generator, as illustrated in Figure 2. As explained in Ref. [33], using a classical discriminator leads to a faster convergence of the loss function in our case. We also stress that the quantum generator is what we eventually want to run extensively after the training: The discriminator network is not useful in the deployment as the target is the generation of synthetic data thanks to the generator, for which we are interested in the possibility of performance improvements using a quantum device.

The classical discriminator is composed of a deep convolutional neural network with 4 convolution layers. The exact details of its implementation can be found in the code [79] which is based on the open-source Python quantum software development kit `qibo` [80].

3.2. Quantum generator of the style-based qGAN and training procedure

The quantum generator of the style-based qGAN is depicted in Figure 3. It is essentially a quantum neural network for a quantum feature map encoding the latent vector (the random noise with a given latent dimension, generated from a standard Gaussian noise distribution) into a quantum state $|\Psi\rangle$. We then perform on this quantum state the

measurement of an expectation value to obtain the fake samples. Each layer of this quantum feature map is comprised of a set of alternating R_y and R_z one-qubit gates followed by a set of entangling gates, that we chose as controlled rotations $c\text{-}R_y$ as explained in Ref. [33]. For our data augmentation experiment we use the same exact hyperparameters as in our previous work: one layer and a latent dimension of five for the latent vector \mathbf{r} . The gate angles follow a simple affine function of both the latent vector and the trainable parameters \mathbf{p} , such that we have

$$R_{y/z}^{l,m}(\mathbf{p}, \mathbf{r}) = R_{y/z}(p^{(l)}r^{(m)} + p^{(l-1)}), \quad (1)$$

with m running from 1 to $D_{lat} = 5$, the latent dimension, and l running from 1 to the total number of trainable parameters, depending on the number of layers and on the number of qubits. This encoding is the quantum equivalent of classical machine learning encoding with weights and biases. The salient feature of the styled-based approach is the encoding of the latent variables all over the network, in a data re-uploading approach.

The last layer of the quantum circuit contains the measurement operator. The final sample $x \in \mathbf{R}^N$, where N is the number of distributions (equivalent to the number of qubits in our data augmentation experiment for the base circuit), is generated as a vector containing the expectation values of individual Pauli Z operators for each qubits over the final state $|\Psi(\mathbf{r})\rangle$ obtained with the circuit of Figure 3,

$$\mathbf{x} = (-\langle\sigma_z^1\rangle, -\langle\sigma_z^2\rangle, \dots, -\langle\sigma_z^N\rangle). \quad (2)$$

We use a minmax pre-processing on the input data, so that the data for each distribution is rescaled within the range $[-1; 1]$, using the power transform from the Python package `scikit learn` [81]. The data points generated by Equation 2 are post-processed through the reverse power transform to obtain the actual generated distributions.

The training procedure for the style-based qGAN is described at length in Ref. [33]. We briefly sketch it in order to introduce the functions we have used for the loss function and for the measure of performance of the quantum generator. We alternately train the discriminator network and the quantum generator network in an adversarial game: The discriminator is improved to distinguish the input (real) training data from the fake data produced by the generator, and then the generator is improved to produce better fake data to trick the discriminator. Both neural networks are trained with binary cross-entropy loss functions. The training is achieved when the Nash equilibrium of the two loss functions is reached:

$$\begin{aligned} \min_{\mathbf{p}_g} \mathcal{L}_G(\mathbf{p}_g, \mathbf{p}_d), \\ \max_{\mathbf{p}_d} \mathcal{L}_D(\mathbf{p}_g, \mathbf{p}_d), \end{aligned} \quad (3)$$

where \mathcal{L}_G is the loss function of the generator, \mathcal{L}_D is the loss function of the discriminator, \mathbf{p}_g and \mathbf{p}_d are the trainable parameters of the generator and the discriminator, respectively.

Our set of real data for the data augmentation experiment is based on high-energy physics, in particular Monte Carlo event generation for the Large Hadron Collider (LHC)

at CERN. We use the same dataset as in Ref. [33], in which the style-based qGAN was proposed, so that we can also compare our data augmentation experiment to the results we obtained before on a different IBM chip. The training data is composed of 10^4 events for the production process $pp \rightarrow t\bar{t}$ at a 13 TeV center-of-mass energy, the production of top-antitop quarks at the LHC in the collision of two protons. We use the computer program MadGraph `MG5_aMC` [82, 83] to produce the training data as well as the 10^5 reference samples to which we compare our generated 10^5 samples. We get a set of three distributions corresponding to physical quantities describing the process: Mandelstam variables s and t (both in giga-electronvolt squared, or GeV^2) and the rapidity y . It is important to note that the s and t distributions, in particular, are highly non-Gaussian distributions. In order to quantify the quality of the generator, we use the Kullback-Leibler divergence (KL) [84]. For two given distributions $P(x)$ and $Q(x)$ of discrete samples x , the KL divergence quantifies how similar these two distributions are,

$$D_{\text{KL}}(P||Q) = \sum_x P(x) \log \left(\frac{P(x)}{Q(x)} \right), \quad (4)$$

which is essentially the difference between the entropy of the distribution $P(x)$ with the cross entropy of $P(x)$ with $Q(x)$. When the two distributions are identical, $D_{\text{KL}} = 0$, so that the smaller the KL divergence is, the more similar the two distributions are.

3.3. Circuit parallelization

Compared to Ref. [33] we have modified the implementation of the quantum generator in several ways. As we want to perform our data augmentation experiment on the latest IBM Heron device as well as on IonQ `aria-1` device, we have updated the Python code to now include qiskit primitive functions instead of `backend.run` calls. We have also reorganized the access to the IBM hardware by using qiskit runtime services. Specifically, we use the Sampler primitive to perform the measurement of the Pauli Z matrix for each qubit, then marginalizing properly on each qubit for the base circuit to obtain the corresponding quantum-measurement output for each physical distribution. This output is then classically post-processed in order to get the final generated physical distributions s , t , or y and their corresponding two-dimensional correlations. We have used qiskit 0.43.1 [85] for generating our results, including also the qiskit-ionq provider* for running on IonQ devices.

In order to profit from the enhanced number of qubits compared to the IBM device used in Ref. [33], we have also implemented a parallelization of the base circuit. The implementation follows from preliminary work performed at the time of Ref. [33]. The idea is to allow for replicating m times the N -qubit base circuit, where N qubits are used to generate N distributions, so that only k/m runs (or k/m samples) are needed to generate k actual samples, at the price of using $m \times N$ qubits for the complete circuit which is run on the hardware.

* <https://github.com/qiskit-community/qiskit-ionq>

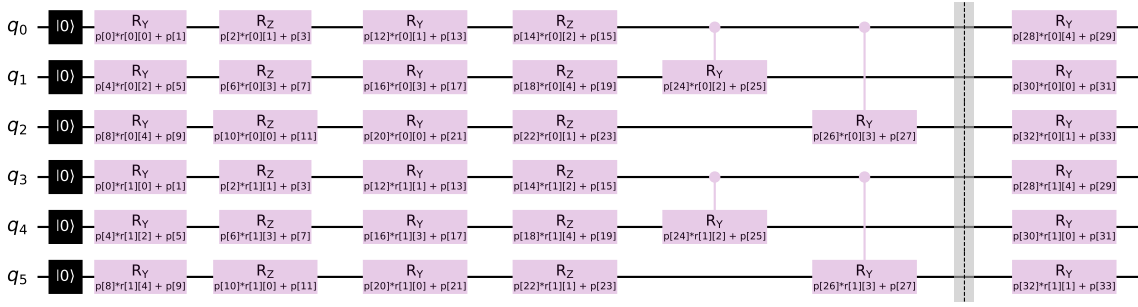


Figure 4. Example of a parallelization of a 3-qubit base circuit of the style-based qGAN with two repetitions, using a total of 6 qubits. Only one layer is used with a (base) latent dimension of five. For simplicity the measurement operations have been omitted.

An example of the method is given in Figure 4 for the case with $m = 2$ and $N = 3$, for our typical generation of 10^5 samples, $k = 100,000$. We have 2 repetitions of the base 3-qubit circuit, allowing for generating only $k/m = 50,000$ samples to get the full set of 10^5 samples. The total number of trainable parameters is the same as for the base circuit with 3 qubits, the base latent dimension is also the same (here $D_{lat} = 5$) but the total latent dimension \ddagger is $m \times D_{lat} = 10$, so that we really have a pair of actual samples generated for each time the circuit is run. In our experiment, we have used 16 repetitions on `ibm_torino` using 48 qubits and 8 repetitions on `aria-1` using 24 qubits, so that we only generated 6250 samples on `ibm_torino` and 12,500 samples on `aria-1` to obtain our full data-augmented sample set. We have used the maximum number of qubits available on `aria-1` for our style-based qGAN experiment. It is in general expected that the higher the number of qubits is used, the smaller the number of samples from the quantum circuit is needed to generate the whole generated sample set, leading to a reduced time spent on the quantum device.

4. Data augmentation results and discussion

We use the quantum generator of our style-based qGAN trained on 10^4 Monte Carlo sample of $pp \rightarrow t\bar{t}$ process at the LHC, as explained in the previous section. In order to also compare to the previous implementation on the IBM `ibmq_santiago` device, which was using a 5-qubit Falcon r4T chip, we have performed the data augmentation experiments on `ibm_torino` and on `aria-1` devices using the same set of trained parameters as in Ref. [33]. The quantum generator consists of one layer of the base 3-qubit circuit displayed in Figure 3, replicated over the whole circuit in order to parallelize the execution as explained in Section. 3.3 and presented in Figure 4.

Each run on the quantum hardware consists of a circuit execution to build the

\ddagger The latent vector \mathbf{r} has been promoted to a latent tensor (r_{ij}) for better readability, with i being the index running over the number of repetitions of the base circuit while j is the index running over the base latent dimension D_{lat} .

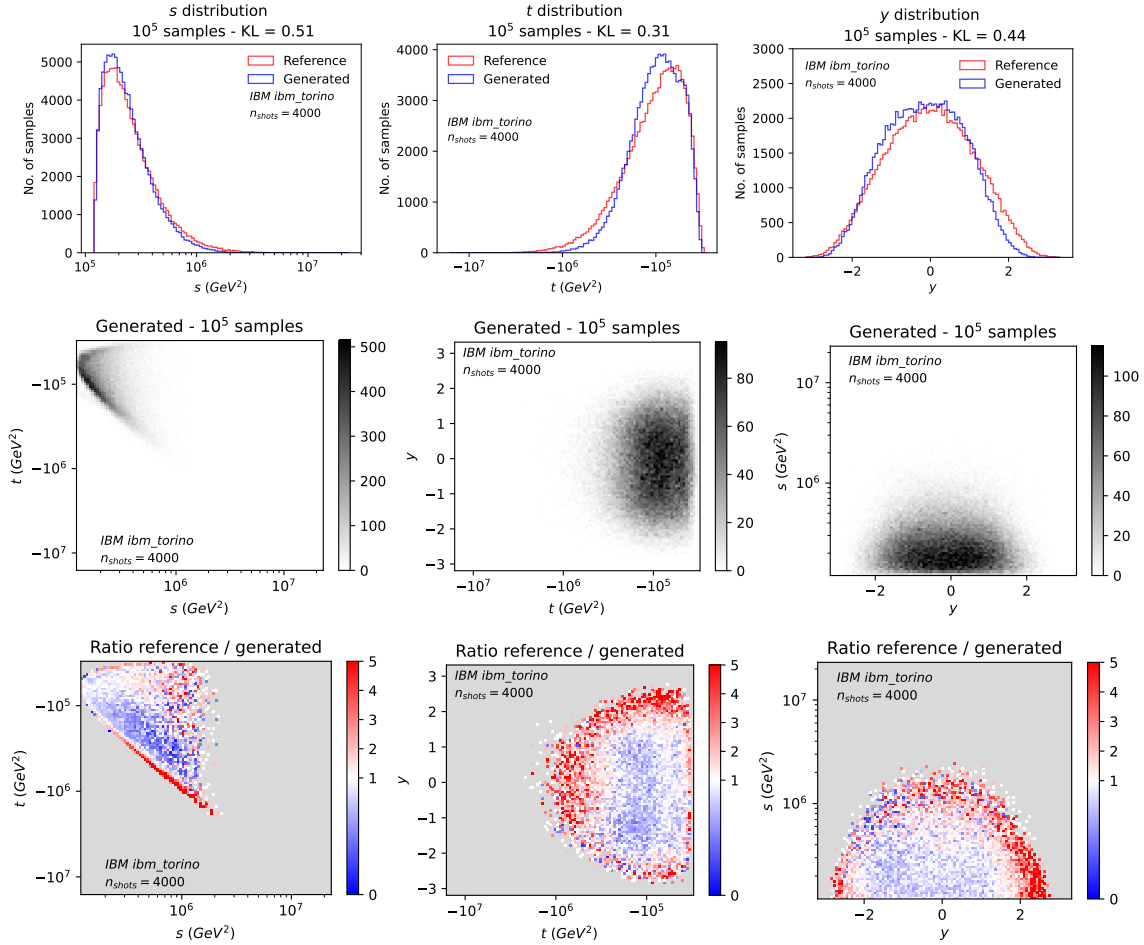


Figure 5. Results for the data augmentation experiment on the IBM `ibm_torino` device using the Heron chip, using the style-based qGAN generator trained with 10^4 samples of Monte Carlo data for the physical observables s, t, y in $pp \rightarrow t\bar{t}$ production at the LHC. Top row: Marginal samples distributions for s, t , and y . Middle row: The corresponding two-dimensional sampling projections. Bottom row: The ratio to the reference underlying prior Monte Carlo distribution. Note that we choose a grey background for the plots at the bottom row to more clearly highlight a ratio of one between reference and generated samples, indicated by white.

quantum state and then a number of measurements (shots) of the Sampler primitive to build the expectation values as displayed in Equation 2. We use $n_{shots} = 4000$ on IBM `ibm_torino` as this is the nominal number of shots on IBM systems. Note that this is a factor of four higher than the number of shots chosen on the IBM `ibmq_santiago` device in Ref. [33]. In principle, the higher n_{shots} is, the less sensitive a quantum experiment is to the statistical error in building the expectation values out of the shots. As IBM systems allow for sending circuits in parallel, for a maximum of 300 circuits, we have performed 22 runs in total to obtain the full set of 10^5 samples: two sessions, each consisting of 10 runs with 300 circuits and one run with 125 circuits.

The amount of time needed for any gate operation on trapped-ion quantum computers is larger than the corresponding timing on superconducting transmon qubits

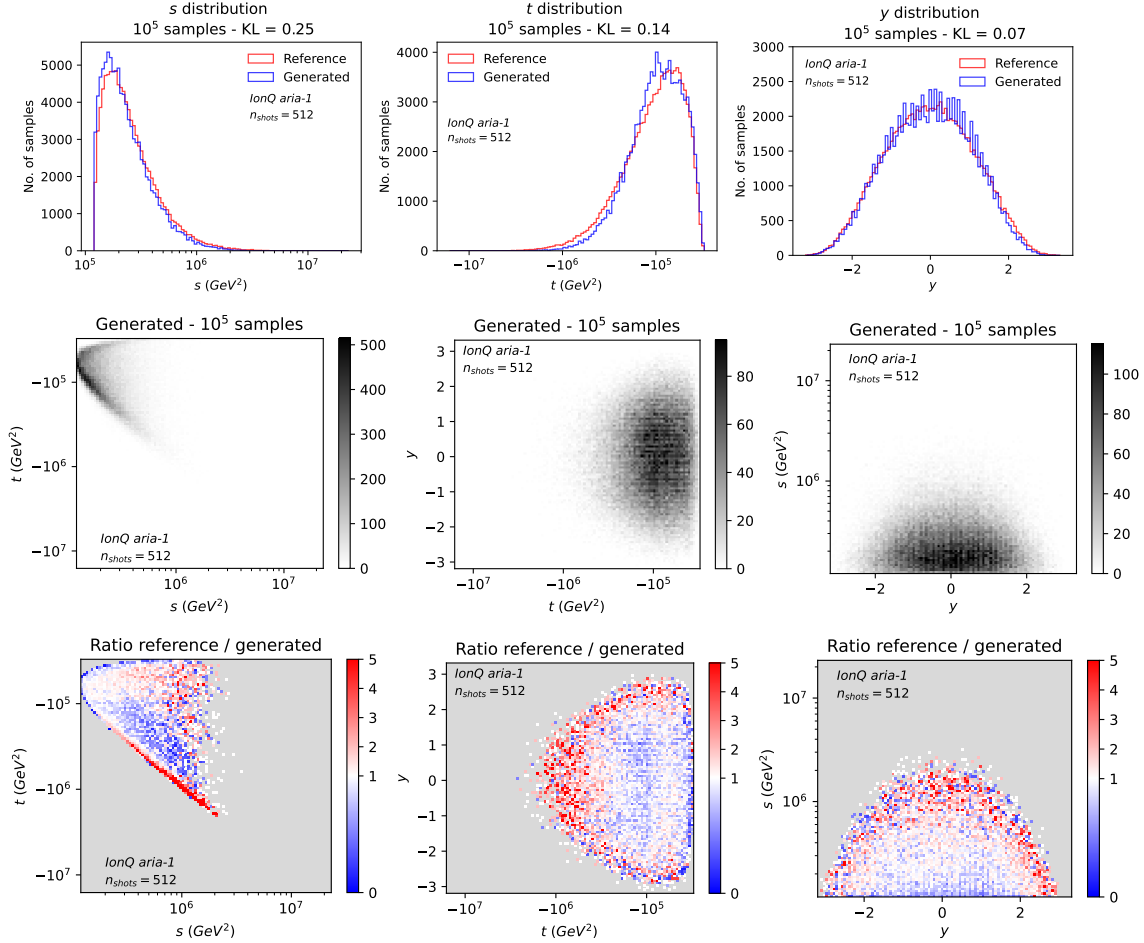


Figure 6. Same as in Figure 5 but for the experiment on the IonQ aria-1 device.

systems as exemplified in Table 1. It is therefore required to choose n_{shots} as small as possible on aria-1, without degrading the quality of the output, while keeping in mind that in general it is possible to choose a smaller number of shots than on superconducting transmon qubits systems because the quality of the qubits is on average higher on trapped-ion computers. We have performed a noise simulation study using aria-1 noise model provided by IonQ with two different values for the number of shots: $n_{shots} = 512$ and $n_{shots} = 1024$. The results are presented in Appendix Appendix A and they lead us to choose $n_{shots} = 512$ for our data augmentation experiment on aria-1. We have performed a total of 12,500 runs on the IonQ aria-1 device as parallel circuit execution is not (yet) available on IonQ systems.

We display in Figure 5 the results of the data augmentation on the IBM ibm_torino devices, with a grid of 100 linearly spaced bins for y and 100 log-spaced bins for s and t . We will use this binning in all of our results. The parallelized circuit built out of the base circuit of Figure 3 is transpiled to the ibm_torino device, which is a step adding more gates in the circuits as: 1) there is no all-to-all connectivity on the Heron chip, resulting in the insertion of swap gates to connect some of the qubits; 2)

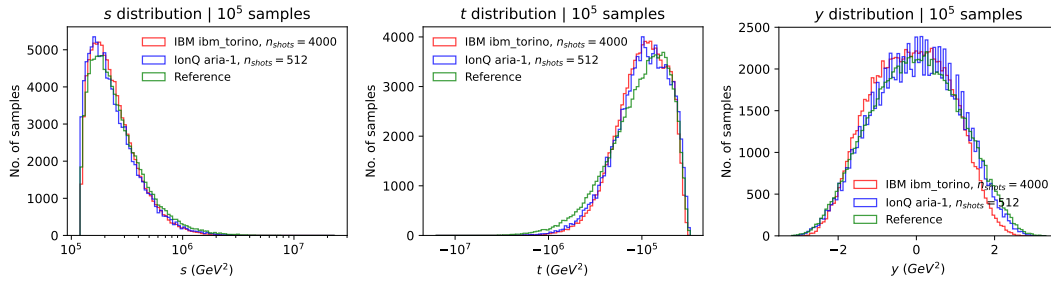


Figure 7. Comparison of the data augmentation on IBM `ibm_torino` (red lines) and on IonQ `aria-1` (blue lines) with the reference sample distribution (green lines) for the marginal samples distributions s , t , and y .

the circuit has to be adapted to the set of native gates of the quantum device. In the top row, we compare the one-dimensional projections of samples generated by the quantum generator of the style-based qGAN with the reference input distribution using 10^5 samples. The KL divergences are small, and quite similar to the corresponding KL divergences in Figure 7 of Ref. [33] obtained on the IBM `ibmq_santiago` device. The s projection is better on `ibm_torino` with a KL divergence of 0.51, while the t and y distributions are slightly worse (KL divergences of 0.31 and 0.44, respectively). The second row of Figure 5 displays the results for the two-dimensional correlations between the three distributions, while the bottom row displays the ratio between the reference samples (10^5 samples) and the samples generated by the style-based qGAN, where the white and light blue points signal regions of excellent agreement. The correlations are better captured on `ibm_torino` than on `ibmq_santiago`. Overall, the results on the IBM `ibm_torino` device show that the data augmentation is performed quite well and that the parallelization of the circuit works.

Our results for the data augmentation on the IonQ `aria-1` device are presented in Figure 6. Note that we have explicitly deactivated debiasing, which is the standard error mitigation technique provided by IonQ on `aria-1` and activated by default, while it is not on the previous `harmony` device. Similar to Figure 5 we present the results for the one-dimensional projections on the top row including the KL divergences comparing the generated samples with the reference samples; the results for the two-dimensional correlations on the middle row; and the ratios to the reference samples on the bottom row. The KL divergences are small, with KLs of 0.25, 0.14, and 0.07 for s , t , and y distributions, respectively. The correlation plots are also good and the ratio plots display a sizable amount of white and light blue points. These results demonstrate that the data augmentation on the IonQ `aria-1` device has been successfully performed. Together with the successful data augmentation on the IBM `ibm_torino` device presented in the previous paragraph, this demonstrates quantitatively, for the first time, that the style-based qGAN can perform data augmentation on two different hardware technologies.

We can now compare the performance of the two hardware devices. The KL divergences on `aria-1` are a factor of two smaller than on `ibm_torino` for the highly

non-Gaussian s and t distributions and a factor of six smaller for the y distribution: 0.25 (0.14) on `aria-1` compared to 0.51 (0.31) on `ibm_torino` for the s (t) distribution, 0.07 on `aria-1` compared to 0.44 on `ibm_torino` for the y distribution. The comparison of the bottom rows of Figures 5 and 6 also shows that the IonQ device captures the correlations slightly better than the IBM device, with more white and light blue points, even if the difference is not that big for the s and t distributions. Overall the accuracy on IonQ `aria-1` is higher than the accuracy on IBM `ibm_torino`, as also exemplified in Figure 7 where the one-dimensional distributions are compared. The red lines are associated to `ibm_torino`, the blue line correspond to `aria-1`, the green lines correspond to the reference data set. In the y distribution, the blue line of `aria-1` is closer to the green reference line than the red line of `ibm_torino`. It should be noted that out of the 48 qubits on `ibm_torino`, the first 24 would be the best the machine can offer when transpiling the quantum circuits to the actual hardware while the remaining 24 are likely to be of less good quality. This contrasts with `aria-1` where only 24 qubits are used. However, we do not expect this difference to lead to a sizable difference in accuracy, as the comparison between the results on `ibmq_santiago` using 3 qubits [33] and the results on `ibm_torino` with 48 qubits shows no sizable difference in accuracy.

It should be noted that only one run has been executed for each device. Ideally multiple runs would have to be executed in order to average the KL divergences over these multiple runs, but this would have required far more resources. However, we have estimated the error on the KL divergences by calculating the sample variance, which we denote here as σ , on the expectation values of Equation 2 and using it as the exploration of the 68% confidence-level interval on the KL divergences. We have generated 11 sets of (s, t, y) distributions out of the post-processing of the sample vector $(x_i + \delta_j \sqrt{\sigma_i})$, where x_i and σ_i are the components of the sample vector \mathbf{x} generated by each run and the components of the corresponding sample variance vector σ , respectively; $\delta_j = -1 + 0.2 * j$, for j running from 0 to 10. Selecting the maximal and minimal KL divergences amongst the 11 sets and comparing them to the nominal KL divergences, we have obtained, on the `ibm_torino` device, KL divergences of $0.51_{-0.07}^{+0.10}$, $0.31_{-0.01}^{+0.07}$, $0.44_{-0.05}^{+0.01}$ for s , t , and y distributions, respectively. The same exercise on the `aria-1` device yields KL divergences of $0.25_{-0.07}^{+0.10}$, $0.14_{-0.05}^{+0.09}$, $0.07_{-0.01}^{+0.06}$ for s , t , and y distributions, respectively. These errors do mitigate the difference in accuracy we observe between the IBM and the IonQ devices, such that the performance on the two devices are actually much closer than expected by looking at only the nominal values of the KL divergences. However, the IonQ device is still more accurate with lower KL divergences.

In order to get more insight into what could drive this difference in accuracy, we have also performed another data augmentation experiment on the IBM `ibm_cusco` device based on the Eagle chip, for which the two-qubit gate error rate is one order of magnitude larger than the error rate on the Heron chip in the `ibm_torino` device, as reported in Table B1 in Appendix Appendix B compared to the specifications of `ibm_torino` presented in Table 1. The results are presented in Appendix Appendix B, demonstrating that overall the accuracy is quite similar, except for the correlation plots

which are much better with `ibm_torino` than with `ibm_cusco`. These results, when compared to the results of `aria-1` device, indicate that the two-qubit error rate has a moderate impact on the accuracy. However, the readout error rate is significantly different between IonQ devices and IBM devices, as presented in Table 1. The one-order-of-magnitude improvement on IonQ `aria-1` compared to IBM `ibm_torino` are likely to explain the difference in accuracy that we observe.

It is quite well known that superconducting qubits have a readout error of the order of 1% whereas the error rate for gate operations can be much lower, see e.g. Ref. [86] where single-qubit gate error rate falls below 10^{-4} . There have been recent improvements in the readout error, see for example Ref. [87] where two-state readout fidelity reached 99.5%. The readout error is part of the more general SPAM error (state preparation and measurement error). A new interesting direction to improve significantly the SPAM error rate on trapped-ion qubits has emerged in the past few years, by replacing ytterbium ions by barium ions $^{137}\text{Ba}^+$. Experiments by IonQ have demonstrated that they can reach a SPAM error rate of only 0.04%†† while Quantinuum has pushed the limit even further by reaching a SPAM error rate of 0.0096% [88]. We expect these radical improvements to have a significant impact not only on the accuracy of (style-based) qGANs, but also on the practical implementation of error correction which relies on repetitive mid-circuit measurements.

We have also recorded the timing of the runs. The timing on `aria-1` is much worse than on `ibm_torino`. This reflects the fact that trapped-ion qubits are significantly slower than superconducting transmon qubits as exemplified in Table 1. The total number of jobs on `aria-1` is 12,500, equivalent to the total number of circuits executed on the device, for an average execution time per job of 17.3 ± 0.5 s, as reported by IonQ. We have executed 512 shots on `aria-1`, so that the average execution time per circuit and per shot is 34 ± 1 ms. The total execution time in order to obtain the full generated sample set on the IonQ quantum computer is 59 hrs, 57 min, 31 s.

On the IBM `ibm_torino` device, however, the total number of jobs is 22 as we can sent parallel multiple circuits in one job. We obtain an average QPU execution time per job and per circuit of 1.078 ± 0.006 s, amounting to an average execution time per job and per circuit, taking into account the various pre- and post-processing steps of the results on the IBM cloud including the transpilation step, of 4 ± 3 s. We have executed 4000 shots on `ibm_torino`, so that the average QPU execution time per circuit and per shot is 0.269 ± 0.002 ms and the average execution time per circuit and per shot is 1.1 ± 0.7 ms. The total execution time in order to obtain the full generated sample set on the IBM quantum computer is 6 hrs, 43 min, 47 s, out of which 1 hr, 52 min 11s on the QPU only.

Comparing the total time spent to obtain the full generated sample set, including the transpilation step, the IBM device is around 8.5 times faster than the IonQ device for the total execution. We should note, however, that the runs on `ibm_torino` have

††See <https://ionq.com/resources/state-preparation-and-measurement-with-barium-qubits>.

been executed with 48 qubits, a parallelization level of 16, requiring in total only 6250 circuits but deeper ones, while the runs on `aria-1` have been executed with 24 qubits, requiring in total twice the amount of circuits. Nonetheless, at the level of a single shot and single circuit execution, the difference is even larger for the execution time including transpilation: around 34 ms on the IonQ device against around 1 ms on the IBM device. This time difference is mitigated by the fact that we required many fewer shots on `aria-1` than on `ibm_torino` in order to obtain our results. Our results are a direct reflection of the sizable difference in the technical specifications reported in Table 1 regarding the time needed for gate operations and measurement readout.

5. Conclusion

Given the significant progress of the quantum hardware we have witnessed in the last years, understanding how different quantum algorithms behave on different types of hardware is of high importance. In this work, we have demonstrated how a key quantum machine learning algorithm, (style-based) qGAN, can not only be implemented but also yield good results on two very different types of hardware.

This demonstration relies on an implementation of the style-based qGAN on two commercially available quantum computers: `ibm_torino` provided by IBM and based on their latest Heron superconducting transmon chip, and `aria-1` system provided by IonQ and based on trapped-ion qubits. Using the same set of real-world data as in Ref. [33] where the style-based qGAN algorithm was introduced, namely the (s, t, y) distributions for $t\bar{t}$ production at the Large Hadron Collider, we have established quantitatively that the style-based qGAN can successfully perform data augmentation on both IonQ `aria-1` and IBM `ibm_torino`, achieving small Kullback-Leibler divergences with a shallow circuit and capturing well the correlations between the three distributions on both architectures. This was hinted in Ref. [33] but a quantitative study was lacking. We also note that we have not used any error mitigation nor suppression techniques, such that a bare comparison of the two hardware architectures is performed as best as we can, owing to the fact that we do not have a perfect control of all operations behind the scene on each machine.

Furthermore, compared to the work in Ref. [33], we have rewritten the code for the quantum generator using modern primitive functions in `qiskit` and we have parallelized the algorithm such that, out of the base circuit with three qubits to represent the three Monte Carlo distributions used as input data for the experiment, we have used up to 24 qubits on `aria-1` and up to 48 qubits on `ibm_torino` to generate 10^5 samples from a training dataset of 10^4 samples. This has allowed us to substantially reduce the amount of actual generated samples out of the quantum generator in order to get the full 10^5 sample set, leading to a substantial speedup of the calculation even if the transpiled circuits on the quantum hardware are deeper, especially on IBM devices because of the lack of all-to-all connectivity of the qubits.

Comparing the performance of the two devices, it has been shown on the one hand

that the two quantum systems deliver good quality results, but the IonQ `aria-1` device achieves a somewhat higher accuracy than IBM `ibm_torino`, in particular for the y distribution but also for the highly non-Gaussian s and t distributions. While the two devices have similar two-qubit gate errors, the readout error rate on the IBM system is one order of magnitude higher than on the IonQ system. Furthermore, the all-to-all connectivity on trapped-ion architecture implies a smaller transpiled circuit compared to the heavy-hex topology on the IBM Heron chip, which in turn means less errors are accumulated until the measurement is performed. These two salient differences between the two hardware architectures are likely to explain the difference in accuracy, even if it should be noted that the results have not been averaged over multiple experiments of generating the 10^5 samples, which could have statistically mitigated a bit the observed difference in accuracy. This would have required a much larger amount of quantum resources. We have chosen instead to translate the sample variance of each run into errors on the calculated KL divergences and have found that while it makes IBM and IonQ devices performing much closer in accuracy, the IonQ device is still delivering more accurate generated distributions. Note again that no error mitigation technique has been used. In particular on IBM machines the readout error, likely driving the difference in accuracy we have observed, can be easily mitigated in order to deliver better quality results.

On the other hand, the execution time on `ibm_torino` is significantly shorter than on `aria-1`, which is due to the significantly faster qubit operations on superconducting transmon qubits than on trapped-ion qubits. Even if the circuits on the IonQ device are shallower as we have used fewer qubits, and even if we have used only 512 shots per circuit on `aria-1` compared to 4000 shots per circuit on `ibm_torino`, in order to speedup the calculation, the total execution time is still around 17 s for one circuit on `aria-1` while it is around 1 s for one circuit on the `ibm_torino` QPU, and of the order of 4 s when including the transpilation step.

We expect that improving the readout error and the coherence time on the IBM Heron chip, as well as the newest more optimized transpilation algorithm, should increase the accuracy of the results on superconducting transmon qubits, not to mention readout error mitigation. A shorter execution time is foreseen on IonQ trapped-ion quantum computer when the gate operations become significantly faster and when the system allows for running multiple circuits in parallel. It is worth noting that improving the readout error rates on IBM systems and the timing of gate operations on IonQ systems are also a requirement for reliable error correction which relies on repetitive mid-circuit measurement.

It would also be interesting to explore in future work the impact of error mitigation and error suppression on the accuracy of the style-based qGAN. While the readout error is easily mitigated, especially on IBM devices, and has a linear scaling, the impact of other error mitigation techniques and of advanced error suppression remains to be explored, as well as the impact of training the style-based qGAN on the quantum hardware to potentially absorb some of the hardware errors as well. A new

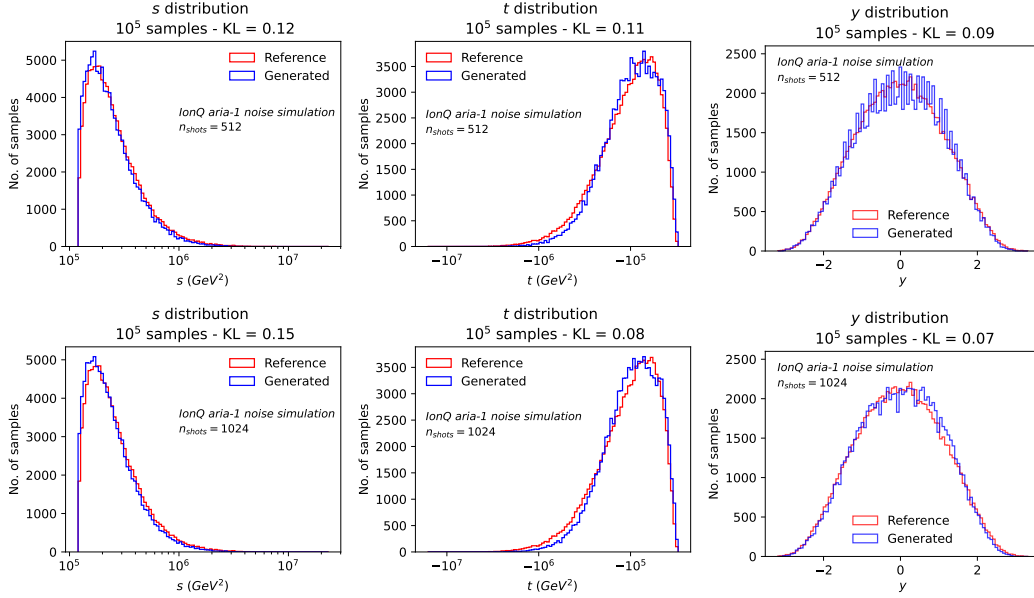


Figure A1. Noise simulation of our data augmentation experiment using the style-based qGAN generator model trained with 10^4 sample of Monte Carlo data for the physical observables s, t, y in $pp \rightarrow t\bar{t}$ production at the LHC, using the noise model of the IonQ *aria-1* device. The results for the marginal distributions are displayed on the top row for 512 shots and on the bottom row for 1024 shots.

implementation of the algorithm using the latest `qiskit 1.0` Estimator primitive is also expected, allowing for scaling the algorithm to a much higher number of qubits used in this work.

Acknowledgments

The author wishes to thank Frederik Flöther and Rajiv Krishnakumar for fruitful discussions, as well as Clément Baglio for his support. The use of IBM Quantum services for this work as well the use of IonQ Compute services are acknowledged. Discussions with the technical supports of IBM and IonQ are also acknowledged. The author declares that there is no conflict of interest.

Appendix A. Noise simulation on IonQ

We have performed two simulations including the *aria-1* noise model in order to assess how many shots were required for the actual run on the IonQ hardware: with 512 shots and with 1024 shots. We present the results in Figures A1, A2, and A3 for the marginal (s, t, y) distribution, the corresponding two-dimensional sampling projections, and the ratio to the reference 10^5 samples, respectively. In each figure the top row displays the results using 512 shots while the bottom row displays the results using 1024 shots.

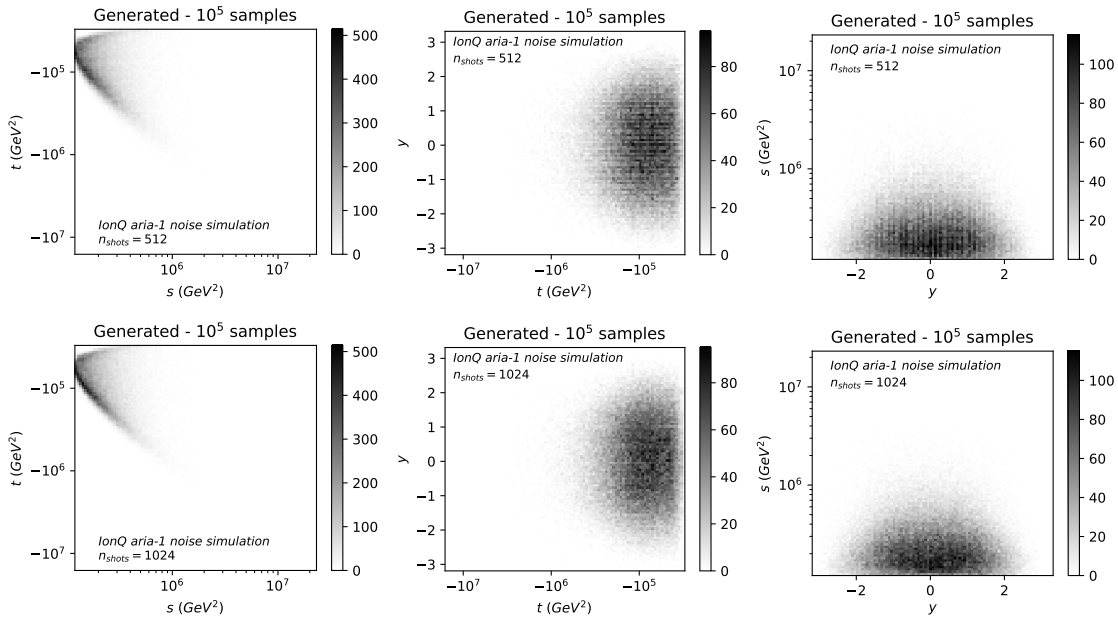


Figure A2. Same as in Figure A1 but for the corresponding two-dimensional sampling projections capturing the correlations between the distributions.

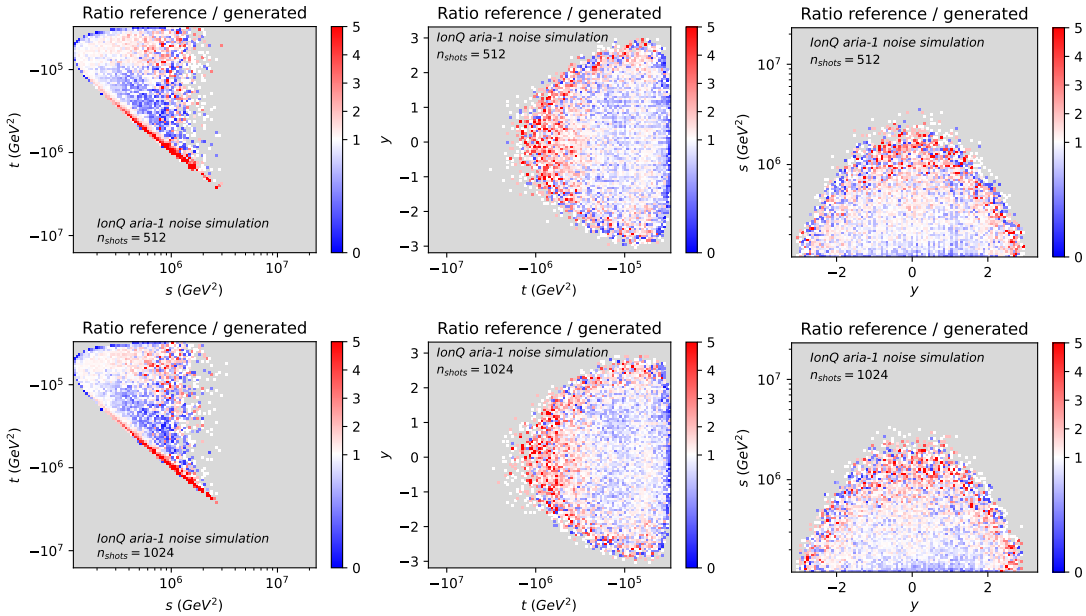


Figure A3. Same as in Figure A2 but for the ratio to the reference underlying prior Monte Carlo distribution. Note that we choose a grey background to highlight when the reference and generated samples are identical.

The KL distances are not significantly different, the two-dimensional sampling distributions are very similar and the ratios to the reference distribution display similar patches of white and light blue points, indicating that the behavior of the simulation does not significantly change from 512 shots to 1024 shots. The noise in the y distribution

| | <code>ibm_cusco</code> |
|--|------------------------|
| # of qubits | 127 |
| Coherence time T_1 (μs) | 131 |
| Coherence time T_2 (μs) | 102 |
| One-qubit gate time (μs) | 0.044 |
| Two-qubit gate time (μs) | 0.487 ^a |
| Readout time (μs) | 4.00 |
| Two-qubit gate error rate | 9.1×10^{-2} |
| Readout error rate | 5.7×10^{-2} |

^aECR gate.

Table B1. List of the most important parameters from the technical specifications of the IBM `ibm_cusco` device using an Eagle chip (average values over all the qubits). The actual values change over time after each calibration of the system and reflect the specifications at the time of our experiment, on October 7th, 2023.

for 512 shots is of statistical nature and does not impact the results of the quantum generator, as indicated by the very similar KL divergences when comparing runs with 512 shots and 1024 shots.

Note that only one run has been performed for each choice of the number of shots, as done also in the hardware runs. Statistics indicates that the typical uncertainty on the quantum measurement with 512 shots is around 8%. To get confidence into the observation of the previous paragraph, we perform the same calculation of the sample variance as in Section 4 for the hardware runs and we obtain, for $n_{shots} = 512$, KL divergences of $0.12^{+0.05}_{-0.04}$, $0.11^{+0.03}_{-0.05}$, $0.09^{+0.01}_{-0.01}$ for s , t , and y distributions, respectively. The same exercise for $n_{shots} = 1024$ results in KL values of $0.15^{+0.04}_{-0.04}$, $0.08^{+0.04}_{-0.02}$, $0.07^{+0.06}_{-0.01}$ for s , t , and y distributions, respectively. These errors do not change the picture of the previous paragraph and we have thus chosen to perform the runs on the actual quantum device using 512 shots to reduce the execution time.

Appendix B. Results on the IBM Eagle `ibm_cusco` quantum system

We have also performed on October 7th, 2023, a run on the 127-qubit `ibm_cusco` device, based on the Eagle chip. The technical specifications given in Table B1 and the comparison with Table 1 show that they are less good than on `ibm_torino`, in particular the one- and two-qubit gate error rates, while the readout error rate is comparable.

The results are displayed in Figure B1. It is quite instructive to compare them to the results obtained with the `ibm_torino` device. The marginal distributions are not significantly different, better for the y distribution on the `ibm_cusco` device while the non-Gaussian t distribution is better on the `ibm_torino` device. This observation indicates that the readout error rate, being the dominant source of error and comparable on both devices, drives the accuracy of the results on IBM systems as far as the marginal one-dimensional distributions are concerned. As the readout error rate is significantly smaller on the IonQ `aria-1` device, the accuracy of the style-based quantum generator is better on the latter.

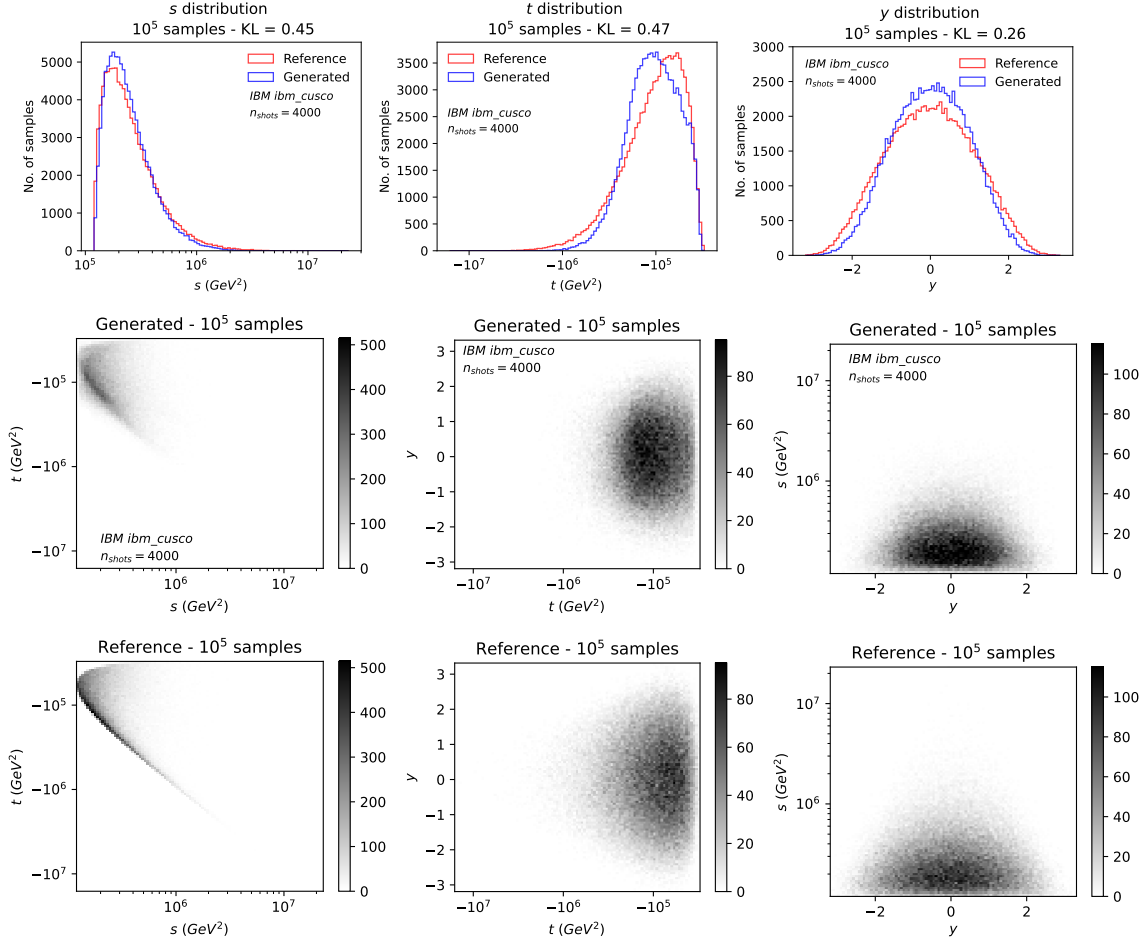


Figure B1. Results for the data augmentation experiment on the IBM `ibm_cusco` device, using the style-based qGAN generator trained with 10^4 samples of Monte Carlo data for the physical observables s, t, y in $pp \rightarrow t\bar{t}$ production at the LHC. Top row: Marginal samples distributions for $s, t,$ and y . Middle row: The corresponding two-dimensional sampling projections. Bottom row: The ratio to the reference underlying prior Monte Carlo distribution. Note that we choose a grey background for the plots at the bottom row to more clearly highlight a ratio of one between reference and generated samples, indicated by white.

However, the comparison of the two-dimensional sampling projections does show a difference between `ibm_cusco` and `ibm_torino`. The `ibm_torino` device produces more accurate projections, as exemplified e.g. by the comparison of the reference $s - t$ projection on the bottom row (left) of Figure B1 with both the $s - t$ projection produced by the `ibm_cusco` device (middle row of Figure B1) and the corresponding projection produced by the `ibm_torino` device (bottom middle row of Figure 5). This reflects the one-order-of-magnitude improvement in the two-qubit gate error rate in the Heron `ibm_torino` device compared to the Eagle `ibm_cusco` device.

References

- [1] Arute F, Arya K, Babbush R, Bacon D, Bardin J C, Barends R, Biswas R, Boixo S, G S L Brandao F, Buell D A *et al.* 2019 *Nature* **574** 505–510 URL <http://doi.org/10.1038/s41586-019-1666-5>
- [2] Zhong H S, Wang H, Deng Y H, Chen M C, Peng L C, Luo Y H, Qin J, Wu D, Ding X, Hu Y *et al.* 2020 *Science* **370** 1460–1463
- [3] Madsen L S, Laudenbach F, Askarani M F, Rortais F, Vincent T, Bulmer J F F, Miatto F M, Neuhaus L, Helt L G, Collins M J *et al.* 2022 *Nature* **606** 75–81 ISSN 1476-4687 URL <https://www.nature.com/articles/s41586-022-04725-x>
- [4] Kim Y, Eddins A, Anand S, Wei K X, van den Berg E, Rosenblatt S, Nayfeh H, Wu Y, Zaletel M, Temme K and Kandala A 2023 *Nature* **618** 500–505 ISSN 1476-4687 URL <https://www.nature.com/articles/s41586-023-06096-3>
- [5] Bluvstein D, Evered S J, Geim A A, Li S H, Zhou H, Manovitz T, Ebadi S, Cain M, Kalinowski M, Hangleiter D *et al.* 2024 *Nature* **626** 58–65 ISSN 1476-4687 URL <https://www.nature.com/articles/s41586-023-06927-3>
- [6] da Silva M P, Ryan-Anderson C, Bello-Rivas J M, Chernoguzov A, Dreiling J M, Foltz C, Frachon F, Gaebler J P, Gatterman T M, Grans-Samuelsson L *et al.* 2024 Demonstration of logical qubits and repeated error correction with better-than-physical error rates (*Preprint* 2404.02280)
- [7] Bravyi S, Cross A W, Gambetta J M, Maslov D, Rall P and Yoder T J 2024 *Nature* **627** 778–782 ISSN 1476-4687 (*Preprint* 2308.07915) URL <https://www.nature.com/articles/s41586-024-07107-7>
- [8] King A D, Nocera A, Rams M M, Dziarmaga J, Wiersema R, Bernoudy W, Raymond J, Kaushal N, Heinsdorf N, Harris R *et al.* 2024 Computational supremacy in quantum simulation (*Preprint* 2403.00910)
- [9] Daley A J, Bloch I, Kokail C, Flannigan S, Pearson N, Troyer M and Zoller P 2022 *Nature* **607** 667–676 ISSN 1476-4687 URL <https://www.nature.com/articles/s41586-022-04940-6>
- [10] King A D, Raymond J, Lanting T, Harris R, Zucca A, Altomare F, Berkley A J, Boothby K, Ejtemaee S, Enderud C *et al.* 2023 *Nature* **617** 61–66 ISSN 1476-4687 URL <https://www.nature.com/articles/s41586-023-05867-2>
- [11] Martínez-Cifuentes J, Fonseca-Romero K M and Quesada N 2023 *Quantum* **7** 1076 ISSN 2521-327X URL <http://dx.doi.org/10.22331/q-2023-08-08-1076>
- [12] Yang T Y and Wang X B 2023 Speeding up the classical simulation of Gaussian boson sampling with limited connectivity (*Preprint* 2311.05355)
- [13] Begušić T, Gray J and Chan G K L 2024 *Science Advances* **10** eadk4321 (*Preprint* 2308.05077) URL <https://www.science.org/doi/abs/10.1126/sciadv.adk4321>

- [14] Kechedzhi K, Isakov S V, Mandrà S, Villalonga B, Mi X, Boixo S and Smelyanskiy V 2024 Effective quantum volume, fidelity and computational cost of noisy quantum processing experiments (*Preprint* 2306.15970)
- [15] Cerezo M, Arrasmith A, Babbush R, Benjamin S C, Endo S, Fujii K, McClean J R, Mitarai K, Yuan X, Cincio L *et al.* 2021 *Nature Reviews Physics* **3** 625–644
- [16] Bharti K, Cervera-Lierta A, Kyaw T H, Haug T, Alperin-Lea S, Anand A, Degroote M, Heimonen H, Kottmann J S, Menke T *et al.* 2022 *Reviews of Modern Physics* **94**(1) 015004 URL <https://link.aps.org/doi/10.1103/RevModPhys.94.015004>
- [17] Dalzell A M, McArdle S, Berta M, Bienias P, Chen C F, Gilyén A, Hann C T, Kastoryano M J, Khabiboulline E T, Kubica A *et al.* 2023 Quantum algorithms: A survey of applications and end-to-end complexities (*Preprint* 2310.03011)
- [18] Biamonte J, Wittek P, Pancotti N, Rebentrost P, Wiebe N and Lloyd S 2017 *Nature* **549** 195–202
- [19] Schuld M and Petruccione F 2018 *Supervised learning with quantum computers* vol 17 (Springer)
- [20] Gujju Y, Matsuo A and Raymond R 2023 Quantum machine learning on near-term quantum devices: Current state of supervised and unsupervised techniques for real-world applications (*Preprint* 2307.00908)
- [21] Amin M H, Andriyash E, Rolfe J, Kulchytskyy B and Melko R 2018 *Phys. Rev. X* **8**(2) 021050 URL <https://link.aps.org/doi/10.1103/PhysRevX.8.021050>
- [22] Liu J G and Wang L 2018 *Phys. Rev. A* **98**(6) 062324 URL <https://link.aps.org/doi/10.1103/PhysRevA.98.062324>
- [23] Benedetti M, Garcia-Pintos D, Perdomo O, Leyton-Ortega V, Nam Y and Perdomo-Ortiz A 2019 *npj Quantum Information* **5** 1–9
- [24] Hamilton K E, Dumitrescu E F and Pooser R C 2019 *Phys. Rev. A* **99** 062323
- [25] Coyle B, Mills D, Danos V and Kashefi E 2020 *npj Quantum Information* **6** 1–11
- [26] Dallaire-Demers P L and Killoran N 2018 *Phys. Rev. A* **98** 012324
- [27] Lloyd S and Weedbrook C 2018 *Phys. Rev. Lett.* **121** 040502
- [28] Zoufal C, Lucchi A and Woerner S 2019 *npj Quantum Information* **5** 1–9
- [29] Hu L, Wu S H, Cai W, Ma Y, Mu X, Xu Y, Wang H, Song Y, Deng D L, Zou C L *et al.* 2019 *Science advances* **5** eaav2761
- [30] Situ H, He Z, Wang Y, Li L and Zheng S 2020 *Information Sciences* **538** 193–208
- [31] Niu M Y, Zlokapa A, Broughton M, Boixo S, Mohseni M, Smelyanskiy V and Neven H 2022 *Phys. Rev. Lett.* **128**(22) 220505 URL <https://link.aps.org/doi/10.1103/PhysRevLett.128.220505>
- [32] Romero J and Aspuru-Guzik A 2021 *Advanced Quantum Technologies* **4** 2000003

- [33] Bravo-Prieto C, Baglio J, Cè M, Francis A, Grabowska D M and Carrazza S 2022 *Quantum* **6** 777 ISSN 2521-327X (*Preprint* 2110.06933) URL <http://dx.doi.org/10.22331/q-2022-08-17-777>
- [34] Chaudhary S, Huembeli P, MacCormack I, Patti T L, Kossaiji J and Galda A 2023 *Quantum Science and Technology* **8** 035002 (*Preprint* 2209.13993)
- [35] Ngo T A, Nguyen T and Thang T C 2023 *Electronics* **12** 856 ISSN 2079-9292 URL <https://www.mdpi.com/2079-9292/12/4/856>
- [36] Benedetti M, Lloyd E, Sack S and Fiorentini M 2019 *Quantum Science and Technology* **4** 043001
- [37] Sim S, Johnson P D and Aspuru-Guzik A 2019 *Advanced Quantum Technologies* **2** 1900070
- [38] Larocca M, Ju N, García-Martín D, Coles P J and Cerezo M 2023 *Nature Computational Science* **3** 542–551 ISSN 2662-8457 (*Preprint* 2109.11676) URL <http://dx.doi.org/10.1038/s43588-023-00467-6>
- [39] Barthe A, Grossi M, Vallecorsa S, Tura J and Dunjko V 2024 Expressivity of parameterized quantum circuits for generative modeling of continuous multivariate distributions (*Preprint* 2402.09848)
- [40] Rudolph M S, Lerch S, Thanasilp S, Kiss O, Vallecorsa S, Grossi M and Holmes Z 2023 Trainability barriers and opportunities in quantum generative modeling (*Preprint* 2305.02881)
- [41] Letcher A, Woerner S and Zoufal C 2024 Tight and efficient gradient bounds for parameterized quantum circuits (*Preprint* 2309.12681)
- [42] Takahashi S, Chen Y and Tanaka-Ishii K 2019 *Physica A: Statistical Mechanics and its Applications* **527** 121261 ISSN 0378-4371 URL <https://www.sciencedirect.com/science/article/pii/S0378437119307277>
- [43] Magnus Wiese Robert Knobloch R K and Kretschmer P 2020 *Quantitative Finance* **20** 1419–1440 URL <https://doi.org/10.1080/14697688.2020.1730426>
- [44] Zhu E Y, Johri S, Bacon D, Esencan M, Kim J, Muir M, Murgai N, Nguyen J, Pienti N, Schouela A, Sosnova K and Wright K 2022 *Phys. Rev. Research* **4** 043092 ISSN 2643-1564 (*Preprint* 2109.06315) URL <http://dx.doi.org/10.1103/PhysRevResearch.4.043092>
- [45] Assouel A, Jacquier A and Kondratyev A 2022 *Quantum Machine Intelligence* **4** 28 (*Preprint* 2110.02742) URL <https://doi.org/10.1007/s42484-022-00083-z>
- [46] Sandfort V, Yan K, Pickhardt P J and Summers R M 2019 *Scientific Reports* **9** 16884 URL <https://doi.org/10.1038/s41598-019-52737-x>
- [47] Biswas A, Nasim M A A, Imran A, Sejuty A T, Fairouz F, Puppala S and Talukder S 2023 Generative adversarial networks for data augmentation (*Preprint* 2306.02019)

- [48] Zhou N R, Zhang T F, Xie X W and Wu J Y 2023 *Signal Processing: Image Communication* **110** 116891 ISSN 0923-5965 URL <https://www.sciencedirect.com/science/article/pii/S0923596522001709>
- [49] Li J, Topaloglu R and Ghosh S 2021 Quantum Generative Models for Small Molecule Drug Discovery (*Preprint* 2101.03438) URL <https://doi.org/10.1109/TQE.2021.3104804>
- [50] Jain P and Ganguly S 2023 *Journal of Emerging Investigators* **6** 1–7 (*Preprint* 2212.07826) URL <https://doi.org/10.59720/22-143>
- [51] Anoshin M, Saginalieva A, Mansell C, Shete V, Pflitsch M and Melnikov A 2023 Hybrid quantum cycle generative adversarial network for small molecule generation (*Preprint* 2402.00014)
- [52] Zeng J, Wu Y, Liu J G, Wang L and Hu J 2019 *Phys. Rev. A* **99** 052306
- [53] Bravyi S, Dial O, Gambetta J M, Gil D and Nazario Z 2022 *Journal of Applied Physics* **132** 160902 ISSN 1089-7550 URL <http://dx.doi.org/10.1063/5.0082975>
- [54] Gold A, Paquette J P, Stockklauser A, Reagor M J, Alam M S, Bestwick A, Didier N, Nersisyan A, Oruc F, Razavi A *et al.* 2021 *npj Quantum Information* **7** 142 (*Preprint* 2102.13293)
- [55] Bernardini F, Chakraborty A and Ordóñez C R 2023 *European Journal of Physics* **45** 013001 URL <https://dx.doi.org/10.1088/1361-6404/ad06be>
- [56] Wright K, Beck K M, Debnath S, Amini J M, Nam Y, Grzesiak N, Chen J S, Piseni N C, Chmielewski M, Collins C *et al.* 2019 *Nature Communications* **10** 5464 (*Preprint* 1903.08181)
- [57] Chen J S, Nielsen E, Ebert M, Inlek V, Wright K, Chaplin V, Maksymov A, Páez E, Poudel A, Maunz P and Gamble J 2023 Benchmarking a trapped-ion quantum computer with 29 algorithmic qubits (*Preprint* 2308.05071)
- [58] Pino J M, Dreiling J M, Figgatt C, Gaebler J P, Moses S A, Allman M S, Baldwin C H, Foss-Feig M, Hayes D, Mayer K, Ryan-Anderson C and Neyenhuis B 2021 *Nature* **592** 209–213 (*Preprint* 2003.01293)
- [59] Ghasemian E, Razminia A and Rostami H 2023 *Quantum Information Processing* **22** 378
- [60] Zhu H, Lin H, Wu S, Luo W, Zhang H, Zhan Y, Wang X, Liu A and Kwok L C 2024 *Information* **15** 95 ISSN 2078-2489 URL <https://www.mdpi.com/2078-2489/15/2/95>
- [61] Henriët L, Béguin L, Signoles A, Lahaye T, Browaeys A, Raymond G O and Jurczak C 2020 *Quantum* **4** 327 ISSN 2521-327X URL <http://dx.doi.org/10.22331/q-2020-09-21-327>
- [62] Albrecht B, Dalyac C, Leclerc L, Ortiz-Gutiérrez L, Thabet S, D’Arcangelo M, Cline J R K, Elfving V E, Lassablière L, Silvério H *et al.* 2023 *Phys. Rev. A* **107** 042615 ISSN 2469-9934 URL <http://dx.doi.org/10.1103/PhysRevA.107.042615>

- [63] Lötstedt E and Yamanouchi K 2024 *Chemical Physics Letters* **836** 140975 ISSN 0009-2614 URL <https://www.sciencedirect.com/science/article/pii/S0009261423006802>
- [64] Riofrío C A, Mitevski O, Jones C, Krellner F, Vučković A, Doetsch J, Klepsch J, Ehmer T and Luckow A 2023 A performance characterization of quantum generative models (*Preprint* 2301.09363)
- [65] Hibat-Allah M, Mauri M, Carrasquilla J and Perdomo-Ortiz A 2024 *Commun Phys* **7** 1–9 ISSN 2399-3650 URL <https://www.nature.com/articles/s42005-024-01552-6>
- [66] Bowles J, Ahmed S and Schuld M 2024 Better than classical? The subtle art of benchmarking quantum machine learning models (*Preprint* 2403.07059)
- [67] Riofrío C A, Mitevski O, Jones C, Krellner F, Vučković A, Doetsch J, Klepsch J, Ehmer T and Luckow A 2024 *ACM Transactions on Quantum Computing* Just Accepted URL <https://doi.org/10.1145/3655027>
- [68] Koch J, Yu T M, Gambetta J, Houck A A, Schuster D I, Majer J, Blais A, Devoret M H, Girvin S M and Schoelkopf R J 2007 *Phys. Rev. A* **76** 042319 ISSN 1094-1622 (*Preprint* cond-mat/0703002) URL <http://dx.doi.org/10.1103/PhysRevA.76.042319>
- [69] Krantz P, Kjaergaard M, Yan F, Orlando T P, Gustavsson S and Oliver W D 2019 *Applied Physics Reviews* **6** 021318 ISSN 1931-9401 (*Preprint* 1904.06560) URL <http://dx.doi.org/10.1063/1.5089550>
- [70] Fritz S, Radtke L, Schneider R, Weides M and Gerthsen D 2019 *Journal of Applied Physics* **125** 165301 ISSN 0021-8979 URL <https://doi.org/10.1063/1.5089871>
- [71] Chow J M, Córcoles A D, Gambetta J M, Rigetti C, Johnson B R, Smolin J A, Rozen J R, Keefe G A, Rothwell M B, Ketchen M B and Steffen M 2011 *Phys. Rev. Lett.* **107**(8) 080502 (*Preprint* 1106.0553) URL <https://link.aps.org/doi/10.1103/PhysRevLett.107.080502>
- [72] Jeffrey E, Sank D, Mutus J Y, White T C, Kelly J, Barends R, Chen Y, Chen Z, Chiaro B, Dunsworth A *et al.* 2014 *Phys. Rev. Lett.* **112**(19) 190504 (*Preprint* 1401.0257) URL <https://link.aps.org/doi/10.1103/PhysRevLett.112.190504>
- [73] Merrill J T and Brown K R 2014 *Progress in Compensating Pulse Sequences for Quantum Computation* (John Wiley & Sons, Ltd) pp 241–294 ISBN 9781118742631 (*Preprint* 1203.6392) URL <https://onlinelibrary.wiley.com/doi/abs/10.1002/9781118742631.ch10>
- [74] Mølmer K and Sørensen A 1999 *Phys. Rev. Lett.* **82** 1835–1838 ISSN 1079-7114 URL <http://dx.doi.org/10.1103/PhysRevLett.82.1835>
- [75] Sørensen A and Mølmer K 2000 *Phys. Rev. A* **62** 022311 ISSN 1094-1622 URL <http://dx.doi.org/10.1103/PhysRevA.62.022311>
- [76] Goodfellow I, Pouget-Abadie J, Mirza M, Xu B, Warde-Farley D, Ozair S, Courville

- A and Bengio Y 2020 *Communications of the ACM* **63** 139–144 ISSN 0001-0782 URL <https://doi.org/10.1145/3422622>
- [77] Farnia F and Ozdaglar A 2020 Do GANs always have nash equilibria? *Proceedings of the 37th International Conference on Machine Learning ICML'20* (JMLR.org) (Preprint 2002.09124) URL <https://dl.acm.org/doi/abs/10.5555/3524938.3525222>
- [78] Moghadam M M, Boroomand B, Jalali M, Zareian A, DaeiJavad A, Manshaei M H and Krunz M 2023 *Artificial Intelligence Review* **56** 9771–9807 (Preprint 2106.06976) URL <https://doi.org/10.1007/s10462-023-10395-6>
- [79] contributors Q 2024 qiboteam/qibo: Qibo 0.2.7
- [80] Efthymiou S, Ramos-Calderer S, Bravo-Prieto C, Pérez-Salinas A, García-Martín D, Garcia-Saez A, Latorre J I and Carrazza S 2021 *Quantum Science and Technology* **7** 015018
- [81] Pedregosa F, Varoquaux G, Gramfort A, Michel V, Thirion B, Grisel O, Blondel M, Prettenhofer P, Weiss R, Dubourg V *et al.* 2011 *Journal of Machine Learning Research* **12** 2825–2830 ISSN 1532-4435 URL <https://dl.acm.org/doi/10.5555/1953048.2078195>
- [82] Alwall J, Frederix R, Frixione S, Hirschi V, Maltoni F, Mattelaer O, Shao H S, Stelzer T, Torrielli P and Zaro M 2014 *Journal of High Energy Physics* **07** 079
- [83] Frederix R, Frixione S, Hirschi V, Pagani D, Shao H S and Zaro M 2018 *Journal of High Energy Physics* **07** 185
- [84] Kullback S and Leibler R A 1951 *The Annals of Mathematical Statistics* **22** 79–86
- [85] Qiskit contributors 2023 Qiskit: An Open-source Framework for Quantum Computing
- [86] Li Z, Liu P, Zhao P, Mi Z, Xu H, Liang X, Su T, Sun W, Xue G, Zhang J N *et al.* 2023 *npj Quantum Information* **9** 111 ISSN 2056-6387 (Preprint 2302.08690) URL <http://dx.doi.org/10.1038/s41534-023-00781-x>
- [87] Chen L, Li H X, Lu Y, Warren C W, Križan C J, Kosen S, Rommel M, Ahmed S, Osman A *et al.* 2023 *npj Quantum Information* **9** 26 ISSN 2056-6387 (Preprint 2208.05879) URL <http://dx.doi.org/10.1038/s41534-023-00689-6>
- [88] An F A, Ransford A, Schaffer A, Sletten L R, Gaebler J, Hostetter J and Vittorini G 2022 *Phys. Rev. Lett.* **129** 130501 ISSN 1079-7114 (Preprint 2203.01920) URL <http://dx.doi.org/10.1103/PhysRevLett.129.130501>